


Interaction between two large particles in a dry granular shear flow

Nathalie Fraysse*

*Université Côte d'Azur, CNRS, Institut de Physique de Nice (INPHYNI), Nice, France*Umberto D'Ortona[†]*Aix-Marseille University, CNRS, Centrale Marseille, M2P2, Marseille, France*Nathalie Thomas[‡]*Aix-Marseille University, CNRS, IUSTI, Marseille, France* (Received 18 July 2023; revised 5 April 2024; accepted 5 May 2024; published 4 June 2024)

The interaction between two large spherical particles, called intruders, in a dry granular flow down an incline is brought to light and studied experimentally and numerically. Several parameters are varied, namely, the size ratio between the intruders and the small flowing particles, the thickness of the granular flow, the incline slope and roughness, and the densities of the intruders with respect to the small-particle density. In all cases, intruders get aligned with the flow. A thorough parametric study shows that a transition occurs between attractive and repulsive regimes of interaction: at steady state, intruders either flow at a defined longitudinal distance, which may be zero with intruders in contact, or stand as far apart as possible. The mean longitudinal and vertical distances between the intruders are found to be tightly linked, with all points plotting the pairs on a single, master curve. The wake and shear effects are shown to control the relative position of the intruders. They may be modulated due to the weight and buoyancy of the intruders, and to local modifications of the collisions between intruders and small flowing particles because of the proximity of the incline bottom or the flow surface.

DOI: [10.1103/PhysRevE.109.064903](https://doi.org/10.1103/PhysRevE.109.064903)**I. INTRODUCTION**

The numerous occurrences in natural and industrial environments of flows of polydisperse dry granular materials have attracted much attention and driven many experimental, numerical, and theoretical studies for a long time [1–3]. Most of these studies deal with mixtures of two sizes of particles of the same density, small size ratios between the large and small particles (smaller than 4, typically), and more or less the same fractions of both species. These conditions lead to the usual granular size segregation pattern, with large particles moving toward the free surface of the flow [4–6] according to the so-called Brazil nut effect. Notwithstanding, it was shown that the opposite takes place for high size ratios and low fractions of large particles, still of the same density as the small particles. The large and, consequently, heavy particles can then push away the small ones and make their way down the flowing granular layer. For instance, a few large particles in a shear flow down a rough incline migrate downward and stabilize near the bottom of the flow for size ratios larger than about 4.5. This phenomenon was called reverse segregation [7–9]. It can be thought of in terms of buoyancy: as the flowing small particles have a volume fraction around 0.6, the density ratio between a large particle and the equivalent volume of the

surrounding small particles having the same density tends to 1.7 for very large particles.

Many investigations of the forces acting on objects immersed in dense granular flows have been performed. These objects are usually static in studies of the drag forces that exert on such obstacles to the flow [10,11], whereas the dynamics of a single intruder free to move has often been addressed in an approach to model granular size or density segregation, in granular flows either driven by gravity [7–9,12–17], or by an externally imposed shear [14,18–21]. The size ratios between the intruder and the small flowing particles are lower than 5 [7–9,13–21] or 6 at the most [17,19] in all these studies, except in [7–9] where size ratios as high as 30 were considered. A few investigations, which focus on the interaction between intruders, consider more than one large particles, either static [10,11] or moving in static granular beds [22,23], in 2D or quasi-2D systems only, apart from a short qualitative insight into 3D systems in [22]. To our knowledge, the interaction between large particles free to move in a 3D dense granular flow at size ratios larger than 6 has never been addressed, even though it is likely to be of great relevance in debris flows and industrial processes.

This situation strongly contrasts with that of particles suspended in fluids. Among other issues, the interaction between sedimenting particles has been studied for long [24–37]. The dynamics of solid spheres settling in a Newtonian fluid has proved to exhibit a rich phenomenology including the drafting-kissing-tumbling behavior [38–40] and may result in peculiar patterns [41–43] in the arrangement

*nathalie.fraysse@univ-cotedazur.fr

†umberto.dortona@cnrs.fr

‡nathalie.thomas@univ-amu.fr

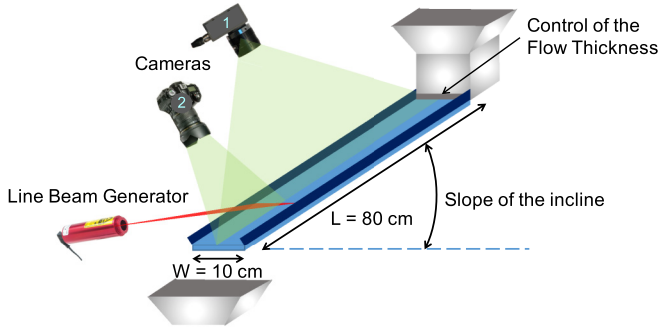


FIG. 1. Sketch of the experimental setup.

of the particles. In sheared suspensions, different migration behaviors are observed depending on the flow conditions and the properties of the particles and of the fluid. Particles may attract or repel each others, which leads to microstructures like trains of particles in channel flows [44–47]. In the case of non-Newtonian fluids, even more complex phenomena may arise, like repulsion between particles for a shear-thickening fluid, or alignment in viscoelastic fluids [48].

In a somewhat similar approach, this work focuses on the dynamics of two large particles (intruders) in a dry granular shear flow made of small particles flowing down a rough incline. Intruders are large and most often in a situation of reverse segregation. Except in a few cases, large and small particles have the same density. Two investigation methods, experimental and numerical, have been implemented. Regarding simulations, the distinct element method (DEM) [49] was used. Its performance makes possible a thorough study of various parameters and gives access to quantities that would be difficult, if not impossible, to measure experimentally. Conversely, experiments provide the necessary validation of the simulation results.

The article is organized as follows. The experimental protocol and the numerical scheme are described in Section II. Section III introduces the physical phenomenon, from both experiments and simulations. Section IV reports a parametric numerical study of the influence of the intruder size, the thickness of the granular flow, the incline slope and roughness, and the intruder densities. A mechanism for the interaction process is proposed and discussed in part V. Section VI ends the article with conclusions.

II. METHODS

A. Experimental protocol

Experiments have been conducted on an 80 cm long and 10 cm wide incline (Fig. 1). The incline is made rough by covering the board with a grade P120 sandpaper. Its slope is set to 23° . Flowing particles are glass beads (density $\rho = 2500 \text{ kg m}^{-3}$) that have been sieved between $300 \mu\text{m}$ and $400 \mu\text{m}$, with a size distribution centered close to $d = 350 \mu\text{m}$. Intruders are colored glass beads (density $\rho = 2580 \text{ kg m}^{-3}$) of same diameter d_i , equal to either 2.0 mm or 3.5 mm, which leads to two size ratios d_i/d of about 6 and 10. A feeding container of an approximate volume of 2 L is placed at the top of the incline. The flow rate from the hopper and thus the

thickness of the granular flow are controlled by the height of the container gate. Its width is kept constant, equal to the channel width. Ambient humidity is kept around 50% relative humidity. After the opening of the container gate, a steady, uniform flow of small glass beads establishes over the entire channel. Soon after, two intruders are gently dropped on the flow, about 10 cm below the gate as the flow thickness might not be constant close to the exit. A homemade injector is used to approximately set the initial relative location of the intruders. The intruders are driven downwards; they rapidly reach their stationary height inside the granular flow, after a few centimeters of travel. A high-resolution video camera with a wide-angle lens, placed above the channel, images its entire length while a digital still camera zooms in on its lower part. The positions of the intruders are obtained from videos recorded at 25 fps typically as well as from photos captured in burst mode. The thickness of the granular flow is measured from the shift of the shadow of a thin tense string or from the deflection of a laser sheet. Flow thicknesses from 2.2 mm to 3.0 mm have been studied experimentally.

B. Numerical model

The numerical method used is the distinct element method (DEM). A linear-spring and viscous damper force model [49,50] is implemented to calculate the normal force between contacting particles. The details on the numerical model and its parameters (normal stiffness, normal damping, collision time, and restitution coefficient) have been published previously and can be found in [9,50,51]. The gravitational acceleration is $g = 9.81 \text{ m s}^{-2}$. The particle properties correspond to those of cellulose acetate: density $\rho = 1308 \text{ kg m}^{-3}$, restitution coefficient $e = 0.87$, and friction coefficient $\mu = 0.7$ [50,52]. In two series of simulations (Sec. IV F), the densities of the intruders are (i) both equally increased or decreased compared to that of the small particles, $\rho_i = \alpha\rho$ with α in the range $[0.35; 2]$, or (ii) modified symmetrically so that the front intruder density is $\rho + \Delta\rho$ and the back intruder density $\rho - \Delta\rho$, with $\Delta\rho$ in the range $[-0.005\rho; 0.15\rho]$. The front intruder is denser, except in a few cases where $\Delta\rho < 0$. Introducing a difference in density between the intruders aims at modifying their relative vertical position in the flow.

To prevent the formation of a close-packed structure, the small particles have a uniform size distribution ranging from $0.95d$ to $1.05d$, with d hereafter referred to as the small-particle diameter. d is equal to 6 mm in the simulations. The large particle diameter is d_i . The collision time is $\Delta t = 10^{-4} \text{ s}$, consistent with previous simulations [52–54] and sufficient for modeling hard spheres [55–57]. These parameters correspond to a stiffness coefficient $k_n = 7.32 \times 10^4 \text{ N m}^{-1}$ [50] and a damping coefficient $\gamma_n = 0.206 \text{ kg s}^{-1}$. The integration time step is $\Delta t/50 = 2 \times 10^{-6} \text{ s}$ to meet the requirement of numerical stability [55].

The initial configuration is obtained as follows. Small beads are placed randomly in the simulation domain, along with two large particles that are placed at $0.75d_i$ above the bottom, aligned at 45° of the flow direction and spaced at twice their diameter from center to center, as illustrated in the left column of Fig. 2. During 0.3 s, gravity is set perpendicular to the bottom plane and particles fall. All beads touching the

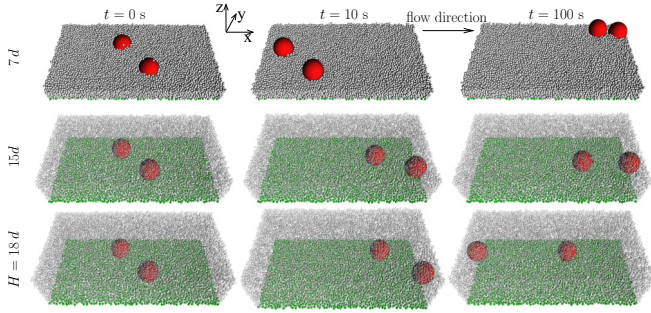


FIG. 2. From the numerical simulations, three successive positions of two intruders (in red) in dry granular flows of small particles (in gray). Particles of the rough incline are green. The size ratio between the large and small particles is $d_i/d = 10$. Three thicknesses of the flow are displayed: $H = 7d$, $15d$, and $18d$. The simulation domain is $80d \times 40d$, and the slope of the incline is 24° . Also see videos 1 to 3 in the Supplemental Material [58].

bottom of the domain stop moving and form a monolayer of bonded particles which generates the roughness of the incline. The other beads will constitute the flowing granular material. The particles of the rough bottom have the same size as the small flowing particles, except for one particular study on the effect of the roughness of the incline, where various diameters of particles, from $d_r = 0.9d$ to $1.6d$, were used to generate the glued monolayer (see Sec. IV E). After 0.3 s, gravity is tilted to the chosen slope (24° , except in Sec. IV D), and the flow starts ($t = 0$ s). Rough-bottom particles are assumed to have an infinite mass for calculation of the collision force between flowing and fixed particles. The velocity-Verlet algorithm is used to update the position, orientation, and linear and angular momenta of each particle. Periodic boundary conditions are applied in the flow direction x and in the transverse direction y of the simulation domain. The size of the domain is $L_x = 80d$ and $L_y = 40d$ in the x and y directions, except in some cases for which the size is increased up to $160d \times 80d$. The positions and velocities of all particles, including the intruders, are stored every 0.1 s for postprocessing purpose. The thickness of the moving granular layer is computed from the surface ($z = 0$) of the roughness of the incline, one small-particle diameter higher than the domain bottom. In Sec. V virtual springs are added between intruders in order to maintain them at defined distances in the x and y directions and facilitate the measurement of the velocity field.

III. RESULTS: EVIDENCE OF AN INTERACTION BETWEEN INTRUDERS

A. First observations

In the first part of the numerical study, all particles have the same density, and the size ratio of the intruder diameter to the small-particle diameter is set to $d_i/d = 10$. This size ratio ensures reverse segregation [7,9]. Three flow thicknesses were implemented ($H = 7d$, $15d$, and $18d$). The equilibrium position of the intruders in the z direction, near the bottom of the granular flow, results from the reverse segregation mechanism and the difficulty to penetrate the lowest small-particle layers where chain forces are efficient enough to support a

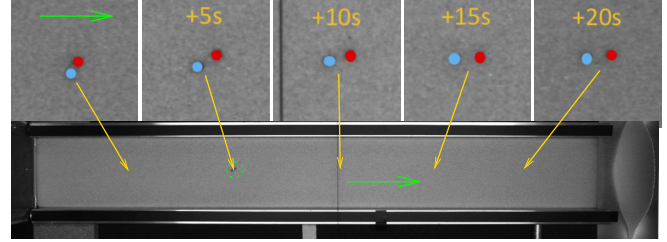


FIG. 3. Pictures from an experiment performed with a granular flow made of small particles of diameter $d \simeq 350 \mu\text{m}$ and two large intruders of diameter $d_i = 2.0 \text{ mm}$, for a size ratio $d_i/d \simeq 6$. The slope of the incline is 23° . The flow thickness is $H = 2.2 \text{ mm} \simeq 6.5d$. The lower picture shows the whole plane, with one location of the intruders highlighted by a green dashed circle as an example. The five upper subimages illustrate the time evolution of the relative position of intruders; the arrows indicate their corresponding locations on the plane. The thick green arrows indicate the direction of the flow. Also see video 4 in the Supplemental Material [58].

large particle. For the thinnest flow, intruders are large enough to emerge from the flow and are visible at its surface. For the two thick flows, intruders are completely embedded in the granular flow, and small particles are drawn partly transparent in Fig. 2 to make the intruders visible. Note that the vertical velocity profile of the flow of small particles down the incline makes the flow very nonuniform over the intruder diameter (shear flow).

The simulations bring to light a striking behavior of the intruders in the granular flow. For the thin flow case ($H = 7d$), they are observed to align in the flowing direction, moving in the wake of the other intruder, and eventually get in contact. Intruders attract each other. For the two thick flow cases, the intruders, initially close, also align but move away from each other, to a distance depending on the flow thickness. For $H = 15d$, intruders locate at a distance (measured from center to center) $\Delta x \simeq 20d$. For $H = 18d$, this distance is $\Delta x \simeq 37d$, which is close to the maximal distance ($\Delta x = 40d$) that can be obtained for periodic boundary conditions and a simulation domain length of $L = 80d$. An increase in the simulation domain length shows that intruders actually repel each other for the thickest flow (see Fig. 8).

A similar qualitative behavior is observed experimentally. Figures 3 and 4 show two experiments performed for the same size ratio ($d_i/d \simeq 6$) and two flow thicknesses. The small beads have a diameter $d \simeq 350 \mu\text{m}$, and the intruder diameter

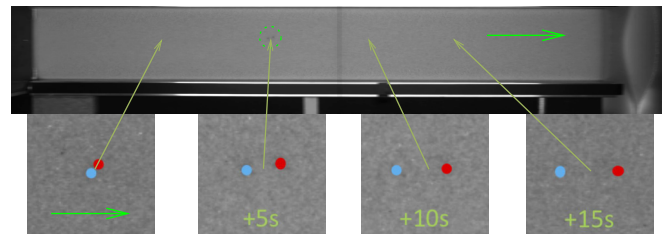


FIG. 4. Same as Fig. 3 for a larger granular flow thickness $H = 2.9 \text{ mm} \simeq 8.5d$. The four lower subimages show the time evolution of the relative position of the intruders. Also see video 5 in the Supplemental Material [58].

is 2.0 mm. The flow thicknesses are $H = 2.2 \text{ mm} \simeq 6.5d$ and $H = 2.9 \text{ mm} \simeq 8.5d$ for Figs. 3 and 4, respectively. Note that the particles flow toward the right in these figures. The subimages display the time evolution of the intruder positions. To facilitate the visualization, their locations are highlighted by two red and blue circles, which have the same diameter as the intruders and stand for the front and back intruders, respectively.

Like in simulations, for both flow thicknesses, the two intruders get aligned with the flowing direction. Intruders, which are initially in contact, move away while flowing. For the thinnest flow (Fig. 3), the intruders eventually locate at a distance $\Delta x \simeq 2.5d_i \simeq 15d$ from center to center. For the thickest flow (Fig. 4), the distance between the intruder centers continuously increases until intruders reach the end of the incline, where the distance comes to $\Delta x \simeq 30d$.

Experiments performed with intruders 3.5 mm in diameter, i.e., a size ratio $d_i/d \simeq 10$, and two flow thicknesses $H \simeq 2.6 \text{ mm} \simeq 7.5d$ and $H \simeq 3.0 \text{ mm} \simeq 9d$, all else being equal, show that intruders also align, but they stay or rapidly come in contact.

Thus, numerical simulations and experiments demonstrate that two large particles in a dry granular flow down an incline do interact. Both approaches suggest that two regimes exist, attractive or repulsive, depending on the thickness of the flow.

B. Time evolution of the relative position of the intruders

The time evolution of the relative position of the two intruders give further details on the process. Figures 5–7 report the longitudinal (Δx , upper curves) and transverse (Δy , lower curves) distances between the intruder centers as a function of time, for the numerical and experimental studies reported above.

As exemplified in Fig. 5, the numerical simulations performed for a size ratio $d_i/d = 10$ show that a stationary regime is reached after a transition period whose duration increases with the flow thickness. The transverse distance (Δy) converges toward zero for all values of the flow thickness, rapidly for a thin flow and more slowly for a thicker flow. Intruders are drawn more or less efficiently into each other's wake (see Sec. V for discussion). Whereas the longitudinal distance (Δx) also converges to a steady state, it exhibits various behaviors of which Fig. 5 gives a representative example. For the thinner flow ($H = 7d$), the longitudinal distance tends to d_i , showing that intruders are almost in contact. For $H = 15d$, the longitudinal distance fluctuates around $\Delta x = 20d$. For the thickest flow ($H = 18d$), the longitudinal distance almost reaches $\Delta x = 40d$, which corresponds to half of the simulation domain length. Due to the periodic boundary conditions used in the simulations, this is the maximum distance that can be reached between two repelling intruders since they interact by both sides of the simulation domain.

Figures 6 and 7 show the time evolution of the longitudinal (Δx , upper curves) and transverse (Δy , lower curves) distances between the two intruder centers in the experiments performed for two size ratios. In Fig. 6, for the size ratio $d_i/d \simeq 10$ and the two small flow thicknesses investigated,

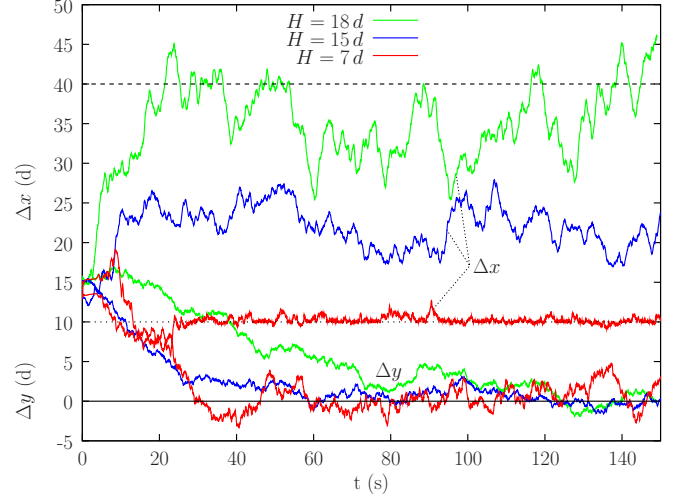


FIG. 5. Longitudinal (Δx , upper curves) and transverse (Δy , lower curves) distances between the two intruder centers ($d_i/d = 10$) measured in small bead diameter (d), as a function of time, for the three flow thicknesses ($H = 7d$, $15d$, and $18d$) of the numerical study corresponding to Fig. 2. The transverse distances Δy converge to zero. The longitudinal distances tend to different values increasing with the flow thickness. The dotted line indicates one intruder diameter $d_i = 10d$, i.e., the minimal longitudinal distance between two intruder centers perfectly aligned with the flow direction. The dashed line ($y = 40d$) corresponds to half of the longitudinal size of the simulation domain, i.e., the maximum distance that two aligned repelling intruders can reach.

the behaviors observed are the same as in the simulations for the thinnest flow. Intruders align and come in contact.

In Fig. 7, for the size ratio $d_i/d \simeq 6$ and a thin flow ($H \simeq 6.5d$, blue curves), the transverse distance Δy also decreases and tends to zero, i.e., intruders get aligned, whereas the longitudinal distance Δx rapidly grows to $10d$, and then

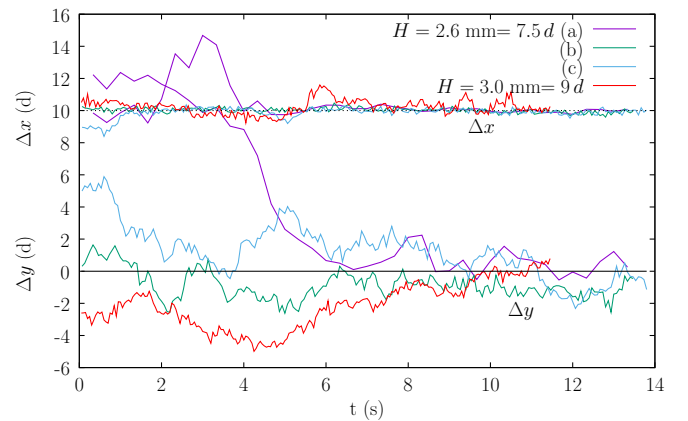


FIG. 6. Longitudinal (Δx , upper curves) and transverse (Δy , lower curves) distances between the two intruder centers measured in small bead diameter (d) for four experiments performed for a size ratio $d_i/d \simeq 10$ and two flow thicknesses $H = 2.6 \text{ mm} \simeq 7.5d$ and $H = 3.0 \text{ mm} \simeq 9d$. The dotted line indicates one intruder diameter $d_i = 10d$, i.e., the minimal longitudinal distance between two intruder centers perfectly aligned with the flow direction.

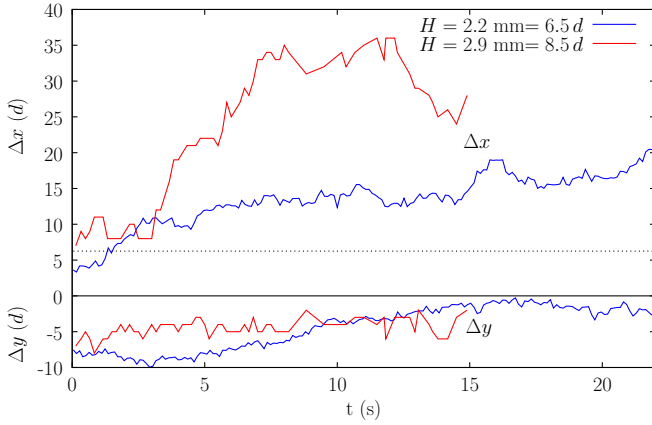


FIG. 7. Longitudinal (Δx , upper curves) and transverse (Δy , lower curves) distances between the two intruder centers measured in small bead diameter (d) for the two experiments corresponding to Figs. 3 and 4, respectively. The size ratio is $d_i/d \simeq 6$, and the flow thicknesses are $H = 2.2 \text{ mm} \simeq 6.5d$ and $2.9 \text{ mm} \simeq 8.5d$. The dotted line indicates one intruder diameter $d_i = 6d$, i.e., the minimal longitudinal distance between two intruder centers perfectly aligned with the flow direction.

reaches some kind of plateau around $15d$, followed by a slight increase which could be due to a nonconstant flow thickness. For the same size ratio $d_i/d \simeq 6$ and a thick flow ($H \simeq 8.5d$, red curves in Fig. 7), the transverse distance Δy also decreases, more slowly than for the thin flow, and does not reach zero before the end of the incline. The longitudinal distance Δx rapidly reaches a value around $\Delta x \simeq 30d$ and fluctuates around it. Note that the curves for the thick case end more rapidly than for the thin case since the flowing velocity increases with the flow thickness. Repeated measurements at a given size ratio and flow thickness (see Fig. 6) show that intruders eventually locate at similar relative positions.

Fluctuations in Fig. 5 draw attention. Regarding the longitudinal distance Δx between intruders, fluctuations grow at increasing flow thickness, from almost null when intruders have come in contact at small flow thickness, to large when intruders are far from one another at large flow thickness. Likewise, in the experiments reported in Figs. 6 and 7, fluctuations on Δx are larger when intruders are far apart than for intruders in contact. Logically, the further the intruders, the weaker the interaction between them and the less their relative position is constrained. Regarding the transverse distance Δy , the amplitude of its fluctuations is rather small in the steady state. Fluctuations on Δy do not show a clear correlation with the thickness of the flow nor with the longitudinal distance.

Finally, it is interesting to note that when intruders are close and not perfectly aligned, they migrate in the transverse direction and towards the front intruder. This is not visible in Fig. 2 due to the periodic boundary conditions but visible in video 1 [58], corresponding to $H = 7d$. When the flow is thick, and intruders are far away, no migration is visible (see videos 2 and 3 [58]). Such a behavior is also observed for particles sedimenting in a fluid: at low Reynolds number, a force which results from hydrodynamic interactions acts along the direction joining the centers of two sedimenting particles,

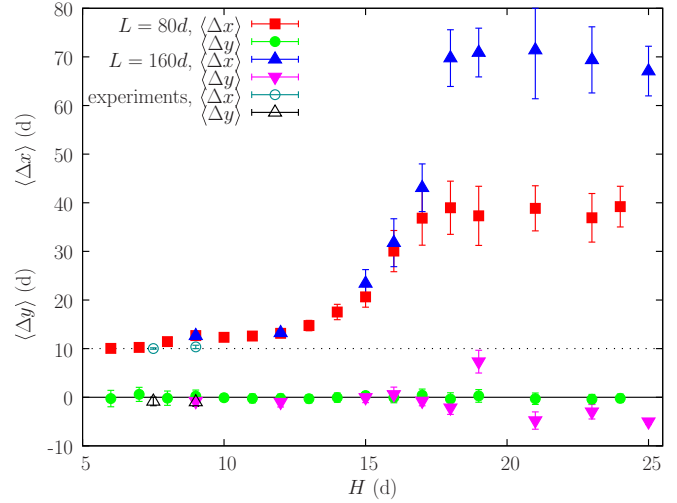


FIG. 8. Mean longitudinal ($\langle \Delta x \rangle$) and transverse ($\langle \Delta y \rangle$) distances (measured from center to center and stated in small-particle diameter d) between two intruders of size ratio $d_i/d = 10$ at increasing flow thicknesses H . In simulations (filled symbols), the domain size is $L_x \times L_y = 80d \times 40d$ (red squares and green circles) or $160d \times 40d$ (blue triangles and magenta reversed triangles). The empty symbols (cyan circles and black triangles) stand for the experiments performed at a size ratio $d_i/d \simeq 10$. The dotted line indicates one intruder diameter $d_i = 10d$, i.e., the minimal longitudinal distance between two aligned intruders.

whose horizontal component induces a lateral drift of the pair of particles [28,35–37]. The study of this phenomenon is ongoing and will be presented in a future work.

C. Numerical study of the steady state

Figures 5–7 confirm the existence of a transition between two regimes of interaction between the intruders, attractive at small flow thickness and repulsive at large flow thickness. This transition can be highlighted by considering the average values computed on the steady state in the numerical simulations.

Figure 8 plots the mean longitudinal ($\langle \Delta x \rangle$) and transverse distances ($\langle \Delta y \rangle$) obtained numerically between the intruder centers, as a function of the flow thickness in the range $H = 6d$ to $25d$, for the size ratio $d_i/d = 10$. The error bars indicate the standard deviation of the distances. To compute the mean, the first 50 s of each simulation are discarded to ensure that the stationary regime has been reached. In a few cases, intruders were not aligned after 50 s and the averaging was started only when intruders got aligned. Averaging is typically performed for a period of 200 s. To probe the effect of periodic boundary conditions, two domain sizes were considered: the size previously used, $80d \times 40d$, was increased to $160d \times 40d$, for a few cases only since simulations become numerically costly for such a large domain.

For all flow thicknesses and both domain sizes, the mean transverse distance ($\langle \Delta y \rangle$) is close to zero, which confirms that intruders initially close ($\Delta x(t=0) = \Delta y(t=0) = \sqrt{2}d_i$) always tend to align with the flow direction by wake effects, as detailed in Sec. V. The mean longitudinal distance ($\langle \Delta x \rangle$) shows a transition around $H = 17d$. Below this thickness,

for both domain sizes, intruders locate at a defined distance that decreases at decreasing flow thickness. This decrease is limited by the size of the intruders since, once aligned, the longitudinal distance between intruders cannot be smaller than one intruder diameter, which corresponds to intruders in contact. In this range of flow thickness smaller than $17d$, the standard deviations are very small, indicating that the attraction between intruders is strong enough not to be sensitive to the fluctuations inherent to a granular flow. Note that the experimental behavior reported in Fig. 6 for a size ratio $d_i/d \simeq 10$ and small flow thickness (empty symbols in Fig. 8) is consistent with the numerical results. In contrast, for large flow thicknesses, the mean longitudinal distance reaches the maximum possible distance considering periodic boundary conditions, i.e., $\langle \Delta x \rangle \simeq 40d$ or $80d$ according to the domain size. Standard deviations are large since longitudinal distances strongly fluctuate in this repulsive regime, as emphasized above.

The almost zero value of the transverse distance at large flow thickness calls for some comments since, in the steady state, intruders are far apart and unlikely to feel each other's wake. Actually, in the simulations, they start to align because they are initially close together, and continue to do so as the longitudinal distance increases, eventually remaining aligned when far apart even though they no longer interact. However, the limited domain size in simulations may also promote the alignment of the intruders. As shown in Fig. 8, two intruders in the repelling regime are better aligned (small error bars for green circles) when artificially held close due to a smaller domain size, while a larger domain leads to larger fluctuations of the transverse distance $\langle \Delta y \rangle$ and mean values as large as $7d$. This may be related to the size of the intruder wakes but also results from the periodic boundary conditions that cause the intruders to meet, and thus realign, from time to time, and more frequently in a smaller domain, which would not happen in an infinite domain.

Figure 8 makes the transition between an attractive and a repulsive regime clear for the size ratio $d_i/d = 10$. To gain a better knowledge on this transition, the size ratio between the intruders and the small particles, the slope of the incline and its roughness, and the densities of the intruders were varied in the numerical simulations. As before, the mean longitudinal and transverse distances are measured for various flow thicknesses. In addition, the vertical locations of the intruders within the granular flow, i.e., their heights above the rough incline, are investigated.

IV. PARAMETRIC STUDY

A. Shift of the transition toward increasing flow thicknesses at increasing size ratio

Three additional size ratios are studied numerically, namely, $d_i/d = 6, 8,$ and 12 . Below a size ratio of 6, intruders undergo a classical surface segregation and are no longer near the bottom of the flow. For size ratios larger than 12, the transition occurs for very large flow thicknesses, and the computational cost strongly increases.

Figure 9 reports the mean transverse and longitudinal distances as a function of the flow thickness. All intruder sizes

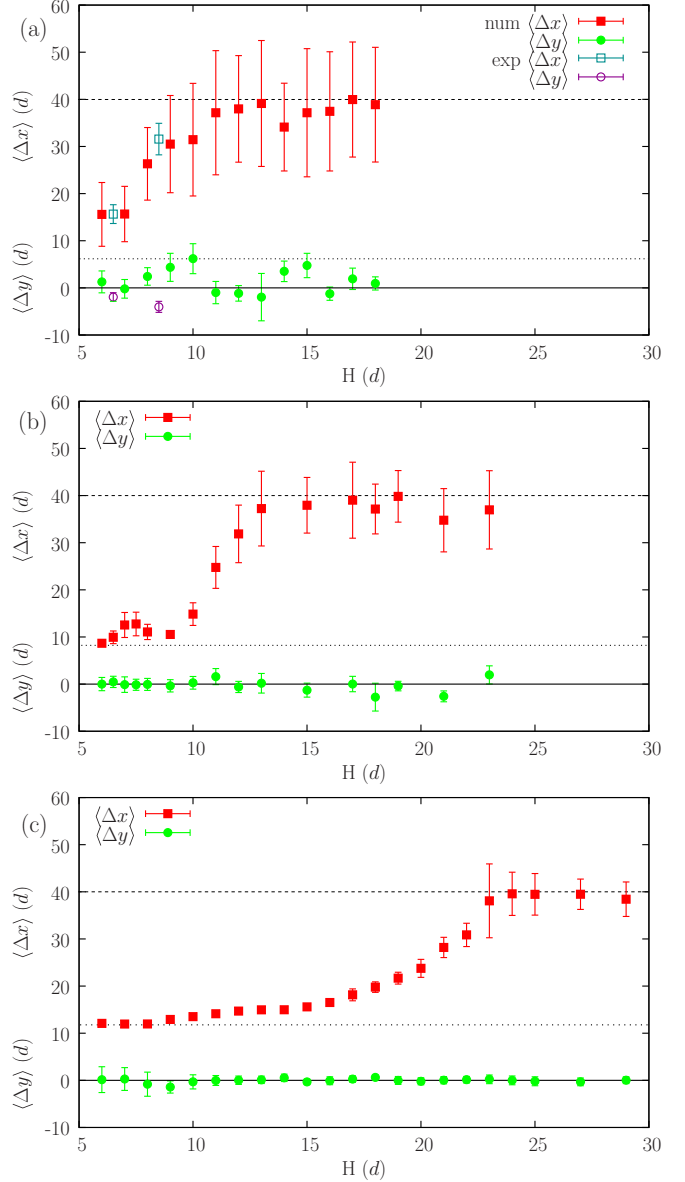


FIG. 9. Mean longitudinal $\langle \Delta x \rangle$ and transverse $\langle \Delta y \rangle$ distances between two intruders at increasing flow thicknesses. The size ratios between intruders and small particles are (a) $d_i/d = 6$, (b) $d_i/d = 8$, and (c) $d_i/d = 12$. The range in flow thickness, starting at $H = 6d$, is adjusted to reach the repulsive regime. The axis scales are kept identical for all graphs to facilitate comparison. All lengths are given in units of small-particle diameter. The dotted lines indicate the intruder diameters. In (a) the empty symbols stand for the experiments performed at $d_i/d \simeq 6$.

lead to the same overall shapes for these curves; however, the repulsive regime is reached at larger flow thickness for larger intruders, around $11d, 13d, 18d,$ and $22d$ for intruders of diameters $d_i = 6d, 8d, 10d,$ and $12d$, respectively. The transition between the attractive and repulsive regimes proves to depend on the intruder size.

Some less important differences between the three graphs in Fig. 9 can be noted. In particular, for the lower size ratio $d_i/d = 6$ [Fig. 9(a)], the mean longitudinal distance always presents a large standard deviation, even for the lowest flow

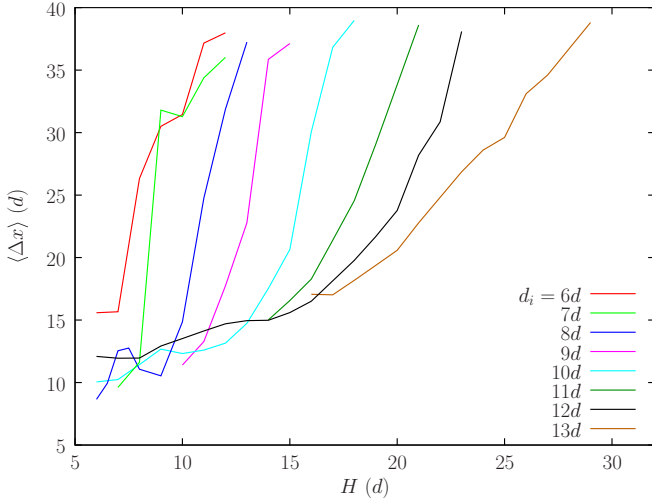


FIG. 10. Mean longitudinal distance $\langle \Delta x \rangle$ vs flow thickness for intruder sizes ranging from $d_i = 6d$ to $13d$. All lengths are given in units of small-particle diameter d .

thicknesses, and the mean transverse distance more or less deviates from zero. The smaller the size difference between the intruders and the small particles, the more the fluctuations inherent to a granular flow outweigh the dynamics of the intruders. In addition, the lower limit of the attractive regime, where intruders are in contact, is not reached at the smallest flow thickness $H = 6d$ reported. This would require to lower the thickness even further. However, this is not possible in the simulations with the chosen parameters since a granular layer thinner than $6d$ does not flow.

The mean longitudinal and transverse distances obtained experimentally for the size ratio $d_i/d \simeq 6$ and for $H \simeq 6.5d$ and $H \simeq 8.5d$ (see Fig. 7) are reported in Fig. 9(a). The agreement with the mean longitudinal distances obtained in simulations, $\Delta x \simeq 16d$ for $H = 6d$ and $\Delta x \simeq 30d$ for $H = 9d$, is noticeable.

Intruders with size ratios $d_i/d = 8$ and 12 [Figs. 9(b) and 9(c)] present similar behavior compared to the case $d_i/d = 10$ (Fig. 8). For thin flows, the intruders attract each other and locate at a defined distance that depends on the flow thickness. For the lower flow thicknesses, the mean longitudinal distance $\langle \Delta x \rangle$ is close to one intruder diameter and intruders are in contact. Standard deviations are small in the attractive regime. For thick flows, intruders repel each other, the mean longitudinal distance $\langle \Delta x \rangle$ is close to $\langle \Delta x \rangle \simeq 40d = L_x/2$ and fluctuations are large.

Similar attractive and repulsive regimes are found for all the size ratios that were explored numerically. Figure 10, where intermediate size ratios $d_i/d = 7, 9, 11$, and 13 are also reported, depicts the attractive-repulsive transition for all the size ratios investigated. Note that the points above the transition have been omitted since the longitudinal distance in the repulsive regime is set by the numerical domain size, around $\Delta x = 40$, and has no physical meaning. The curves of the mean longitudinal distance vs flow thickness all present a similar shape; however, the transition is seen to shift toward higher values of flow thickness and become smoother and smoother as the intruder size increases. For example, for the

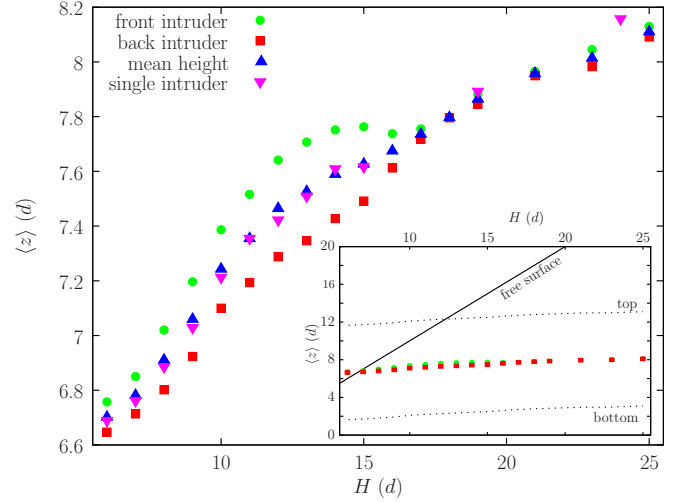


FIG. 11. Mean vertical positions of the front (green circles) and back (red squares) intruders ($d_i = 10d$) vs flow thickness H . The center of mass of the two intruders (blue triangle) as well as the vertical position of one single intruder in a similar flow (magenta reversed triangle) are also plotted for comparison. All lengths are given in units of small-particle diameter. $z = 0$ corresponds to the surface of the rough incline, defined by the summit of the small glued particles (see Sec. II B)). The insert zooms out to visualize the vertical positions of the front-intruder top and bottom (dotted lines) compared to the free surface (solid line) of the granular flow.

size ratio $d_i/d = 8$, an increase in flow thickness from $H = 9d$ to $H = 13d$ is enough to switch from intruders in contact to the repulsive regime, while for the size ratio $d_i/d = 12$, an increase in flow thickness from $H = 15d$ to $H = 23d$ is necessary. A practical consequence is that using large intruders makes it easier to differentiate the various regimes. However, this requires thick granular flows that are numerically expensive and complex to generate experimentally.

B. Vertical locations of the intruders

Numerical simulations also give access to the vertical location of the intruders within the granular flow, hereafter called height of the intruders for simplicity. Figure 11 plots the mean heights of the two intruders above the rough incline ($z = 0$), for the size ratio $d_i/d = 10$ and various flow thicknesses. Note that compared to previous graphs, the vertical axis is strongly stretched.

The main feature of Fig. 11 is that, whereas both intruders adopt an identical vertical position in the flow at flow thickness larger than $18d$, the front intruder stabilizes higher than the back intruder when the flow thickness becomes smaller than $18d$. Figure 8 shows that the value $H = 18d$ corresponds to the transition between the two regimes of interaction for the size ratio $d_i/d = 10$. More specifically, the interaction between the intruders becomes purely repulsive above this value. Since intruders are far from each other, they no longer alter the flow in the vicinity of the other intruder and their heights are identical. Below the value $H = 18d$, Fig. 11 shows that the mean height difference between the intruders $\langle \Delta z \rangle$ increases when the flow thickness decreases to $H = 13d$, then decreases again as the thickness further decreases from $H = 13d$ to

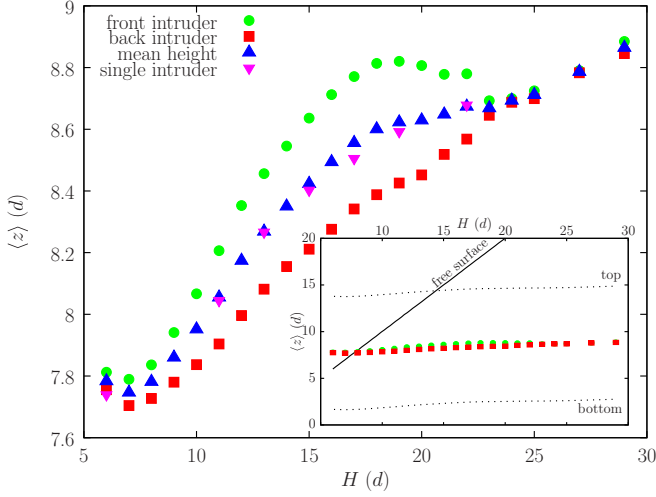


FIG. 12. Same as Fig. 11 for an intruder size $d_i = 12d$.

$H = 6d$ (also see Fig. 13). Figure 12 shows that the same phenomena occur for intruders of size $d_i/d = 12$ but for larger flow thicknesses. The intruders flow at the same height at large flow thickness, down to $H \simeq 23d$, which corresponds to the attractive-repulsive transition for this size ratio [Fig. 9(c); also see Fig. 13]. The mean height difference between intruders increases for flow thicknesses decreasing further, to $H = 16d$, then starts to decrease.

The insets of Figs. 11 and 12 present the positions of the summit, center, and bottom of the front intruder, as well as the location of the free surface of the flow. The mean vertical position of the back intruder is also reported to highlight that the height difference between the two intruders $\langle \Delta z \rangle$ is extremely small, less than half of a small particle diameter. The top dotted line intersects the free surface line for a flow thickness $H \simeq 13d$ for the intruder size $d_i/d = 10$ and $H \simeq 14.5d$ for $d_i/d = 12$. These values are close to those for which the height difference between the intruders starts to decrease. This shows that the decrease in the height difference occurs when the intruders get close to the free surface and eventually start to emerge from the granular flow, with a larger and larger emerged part when the flow thickness decreases further. Conversely, intruders are fully immersed for flows with larger thickness.

Since the intruders are closer and closer as the flow thickness decreases (see Figs. 8 and 9), their interaction strengthens and a larger effect on their height difference $\langle \Delta z \rangle$ is expected. For flow thicknesses smaller than $13d$ ($d_i/d = 10$) or $14.5d$ ($d_i/d = 12$), an extra buoyancy due to the emerging part of the intruders counterbalances the interaction between intruders and reduces the resulting height difference between them, more and more as the emerged part grows. This can explain the decrease in height difference observed at decreasing thickness from about $H = 13d$ in Fig. 11 and $H = 16d$ in Fig. 12.

Figures 11 and 12 call for two more comments. The center of mass of the two intruders as well as the vertical position of one single intruder in a similar flow are also plotted. This shows that, for all flow thicknesses, the center of mass of the two intruders approximately coincides with the vertical location of one single intruder in simulations performed at the

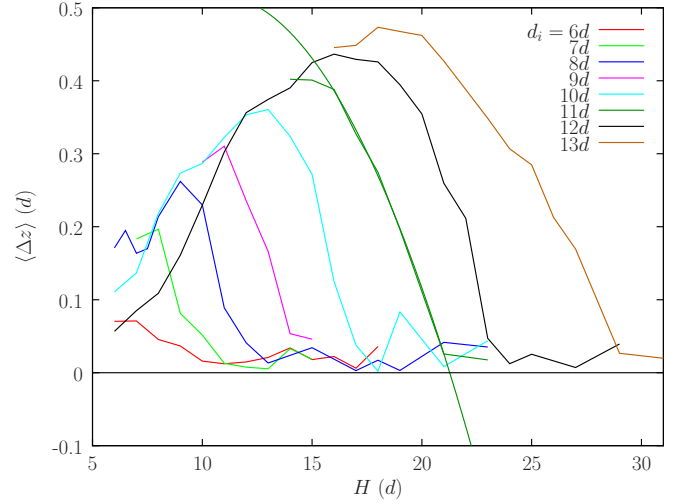


FIG. 13. Mean intruder height difference $\langle \Delta z \rangle$ vs flow thickness H for intruder size ranging from $d_i = 6d$ to $13d$. For the size ratio $d_i/d = 11$, a second-order polynomial fitted on the descending part of the graph is shown. The intersection of this fit with the horizontal axis is used to define the transition thickness H^* . All lengths are given in units of small-particle diameter.

same flow thickness. This is expected at large flow thickness when intruders are far apart and flow at the same height, but this remains valid at small flow thickness when a height difference between the intruders is observed. Thus, the attractive interaction between the intruders causes a lift of the front intruder and a sink of the back intruder while their center of mass settles at a vertical position very close to that of a single intruder.

The second remark relates to the intruder height above the rough bottom. The bottom dotted line in the inset of Fig. 11 gives the position of the front-intruder bottom and shows that, even though intruders are in a reversed-segregated location, they do not touch the rough incline ($z = 0$). A layer of small particles, two to three small-particle diameters thick, flows under the intruder bottom. Its thickness slightly increases with the flow thickness. The same phenomenon is observed for the intruder size $d_i/d = 12$ (Fig. 12).

C. A criterion to define the transition thickness

Figure 13 reports the mean height difference $\langle \Delta z \rangle$ between the front and back intruders as a function of the flow thickness, for intruder sizes ranging from $d_i = 6d$ to $13d$. At decreasing flow thickness, all curves display an increase of $\langle \Delta z \rangle$ followed by a decrease when intruders are emerging. Accordingly, the maximum of the curve shifts towards low flow thicknesses for decreasing intruder sizes. For the case $d_i = 6d$, this decrease does not appear in Fig. 13 as it would start at a flow thickness that is too small for the flow to occur in the simulation.

The intruder height difference conveniently provides an unambiguous mean to define the transition between the attractive and the repulsive regimes. As illustrated in Fig. 13 for the size ratio $d_i/d = 11$, the intersection with the horizontal axis ($\langle \Delta z \rangle = 0$) of a second-order polynomial fit of the decreasing part of the curve gives a value of the flow thickness beyond which the interaction between intruders is purely repulsive

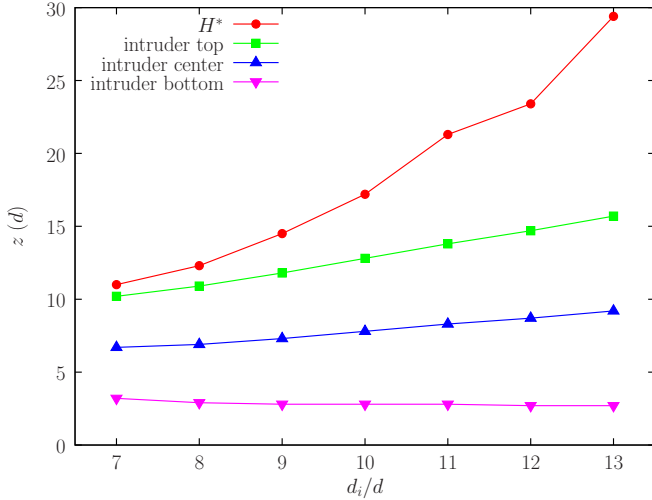


FIG. 14. Transition flow thickness H^* based on the intruder height difference vs intruder size ratio d_i/d (red dots). The mean vertical locations of the intruder summit (green squares), center (blue triangles), and bottom (magenta reversed triangle) for a flow of thickness H^* are also displayed.

and both intruders have the same height. This value is called the transition thickness, noted H^* . For $d_i/d = 11$, the transition thickness is $H^* = 21.3d$. The change in regime, i.e., the transition between attraction and repulsion, is assigned to the flow thickness H^* . Figure 14 summarizes the results for all size ratios. In addition to the transition flow thickness H^* , the mean vertical locations of the intruder summit, center, and bottom for a flow of thickness H^* are also reported. These vertical locations have been obtained by interpolation of previous results since flows with the exact flow thickness H^* have not been simulated. As the intruder vertical location varies very weakly with the flow thickness (see inset of Fig. 11), the interpolation gives accurate results. Figure 14 reports the center of mass of both intruders, but the intruder height difference is so small that using the front or the back intruder gives nearly the same graph.

The comparison of the transition thickness H^* with the position of the intruder summit proves that the attractive/repulsive transition is not concomitant with the emergence of the intruders from the flow. Both intruders are fully embedded for a flow thickness H^* . Furthermore, Fig. 14 shows that the transition thickness increases faster than the height of the intruders. The number of small flowing particles above the intruders at the transition is not constant with the size ratio d_i/d , nor proportional to d_i/d , but strongly increases, while the layer thickness of small particles between the intruder bottom and the rough incline slightly decreases.

Other criteria to define the transition thickness have been tested, for example, the intersection with the horizontal line $\Delta z = 0.05d$, in Fig. 13. Figure 14 remains almost identical for all criteria, and the conclusions are unchanged.

The mechanisms involved in the alignment and the defined longitudinal distance between intruders could be discussed at that point. We choose to postpone them and first explore the influence of other parameters (Secs. IV D to IV F), but the reader may skip these parts and proceed directly to Sec. IV G.

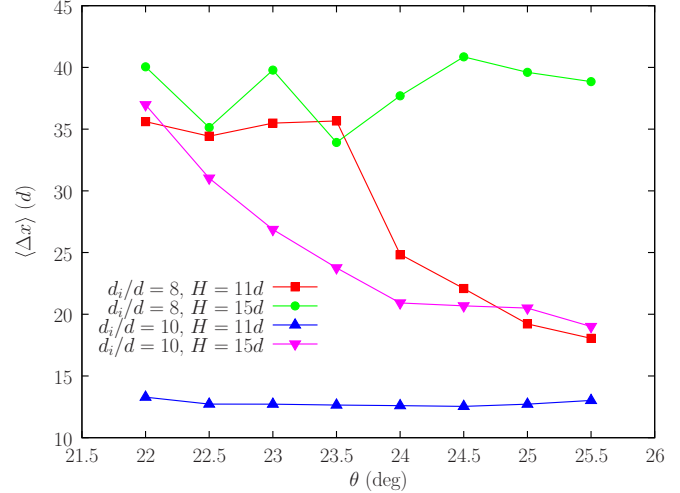


FIG. 15. Mean longitudinal distance $\langle \Delta x \rangle$ between two intruders vs slope: (red squares) $d_i/d = 8$ and $H = 11d$, (green circles) $d_i/d = 8$ and $H = 15d$, (blue triangles) $d_i/d = 10$ and $H = 11d$, and (magenta reversed triangles) $d_i/d = 10$ and $H = 15d$.

D. Slope of the incline

The influence of the slope of the incline is now studied. Whereas previous results were all obtained for an angle of 24° , the incline angle θ is varied from 22° to 25.5° for four typical cases: an attractive case ($d_i/d = 10, H = 11d$) where intruders are almost in contact ($\langle \Delta x \rangle \simeq d_i$), a repulsive case ($d_i/d = 8, H = 15d$) where intruders locate at their maximal distance ($\langle \Delta x \rangle \simeq 40d$), and two intermediate situations ($d_i/d = 10, H = 15d$ and $d_i/d = 8, H = 11d$) where intruders are in an attractive regime, not far from the attractive-repulsive transition, and locate at an intermediate distance.

Figure 15 reports the mean longitudinal distance between intruders, $\langle \Delta x \rangle$, vs slope angle for the four cases. For the two utmost cases, either attractive or repulsive, the variation in slope does not alter significantly the distance between intruders. For the two intermediate cases, increasing the slope angle favors the attractive regime and, conversely, decreasing the slope angle favors the repulsive regime. For the intruder diameter $d_i = 8d$, the transition is sharp and occurs between 23.5° and 24.5° while for the larger intruder diameter $d_i = 10d$, the transition is more progressive and occurs between 22° and 24° . This is reminiscent of the smoothing that is observed at increasing size ratio d_i/d for the transition in $\langle \Delta x \rangle$ with the flow thickness (see Fig. 10).

Figure 16 reports the mean height difference between intruders, $\langle \Delta z \rangle$, vs slope angle, for the same four cases. Apart from the difference in vertical scale, Fig. 16 is close to what one would obtain by mirroring Fig. 15 in the horizontal axis. When the system evolves toward the attractive regime at increasing slope angle, the longitudinal distance between intruders decreases, and, simultaneously, the difference in height of the intruders increases.

On the whole, a variation in the angle of the incline has a rather weak impact on the attractive-repulsive transition and causes the intruders to switch from one regime to the other only when the system is already close to the

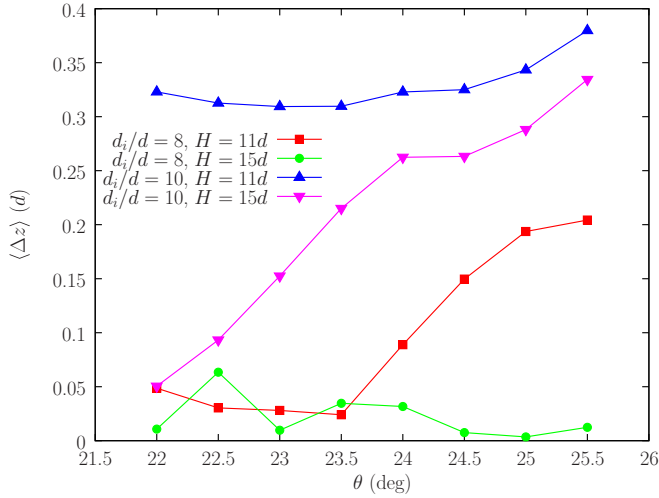


FIG. 16. Mean height difference $\langle \Delta z \rangle$ between two intruders vs slope: (red squares) $d_i/d = 8$ and $H = 11d$, (green circles) $d_i/d = 8$ and $H = 15d$, (blue triangles) $d_i/d = 10$ and $H = 11d$, and (magenta reversed triangles) $d_i/d = 10$ and $H = 15d$.

transition. Nevertheless, increasing the slope favors the attracting regime and, as a consequence, increases the transition thickness H^* .

E. Incline roughness

The roughness of the incline is now varied, for an incline angle of 24° , a size ratio $d_i/d = 10$, and a flow thickness $H = 15d$, one of the two previous intermediate case where intruders locate at a defined distance, in an attractive regime not far from the attractive-repulsive transition. Up to now, the incline was made rough with glued particles of the same size as the small flowing particles d . Here inclines whose roughness is created with glued particles of size ranging from $d_r = 0.9d$ to $1.6d$ are investigated. An incline made rough with smaller particles, namely, $d_r = 0.8d$, leads to a mean velocity of the flow, which is extremely high, indicating that a slip occurs at the base of the flowing material. On the other hand, the roughness obtained with particles of size $d_r = 1.5d$ is known to generate the highest friction for a granular flow made of particle of size d [59], and the actual roughness of the incline is expected to decrease when larger particles are used because flowing particles fill the voids between them.

Figure 17 reports the mean longitudinal distance, $\langle \Delta x \rangle$ (red squares, left axis), and the mean height difference, $\langle \Delta z \rangle$ (blue triangles, right axis), between the intruders with respect to the incline roughness, expressed by means of the size of the glued particles. A decrease in the size of the glued particles, i.e., a decrease in roughness, causes the system to evolve toward the attractive regime: the distance between intruders decreases, and, simultaneously, the difference in height of the intruders increases. The variations in longitudinal distance $\langle \Delta x \rangle$ and height difference $\langle \Delta z \rangle$ between intruders with incline roughness being moderate, averaging over 500 s was necessary to obtain statistically significant mean values.

It can be noted that both increasing the incline angle and decreasing the incline roughness result in a shift toward the attractive regime while implying an increase in the mean flow

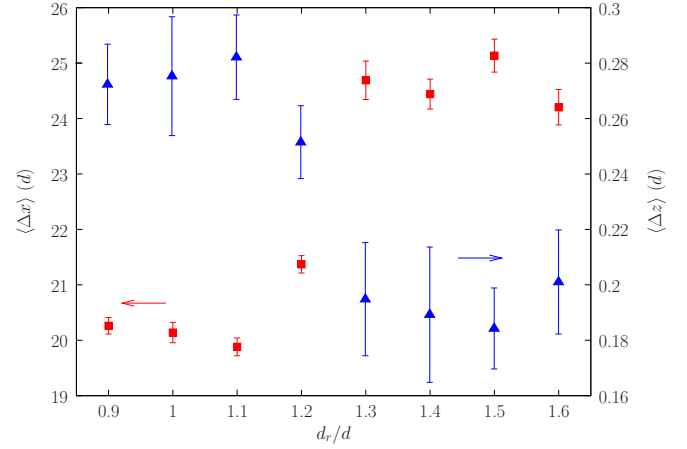


FIG. 17. Mean longitudinal distance $\langle \Delta x \rangle$ (red squares, scale on left axis) and mean height difference $\langle \Delta z \rangle$ (blue triangles, scale on right axis) between intruders vs incline roughness expressed by means of the size of the glued particles, from $d_r = 0.9d$ to $1.6d$. The intruder size is $d_i/d = 10$, the flow thickness $H = 15d$, and the incline angle $\theta = 24^\circ$. Error bars show a 95% interval of confidence of the mean value.

velocity. This can be used to get an estimate of the relative impact of these two parameters. The above variation in the incline roughness yields an increase in $\langle \Delta x \rangle$ around $4d$, while the mean flow velocity is observed to decrease by a factor 1.2. The variation in the slope angle from 22° to 25.5° yields a decrease in $\langle \Delta x \rangle$ around $18d$, more than 4 times larger, while the mean flow velocity is observed to increase by a factor 4.3 only. Therefore, in terms of variations of longitudinal distance vs flow velocity, the incline roughness has a slightly weaker effect than the incline angle.

F. Changing intruder densities

To further explore the reciprocal link that is highlighted by the above between the longitudinal and the vertical distances between intruders, the densities of the intruders are modified in two different ways. First, since a difference in density between the intruders should alter distinctively their heights in the flow and thus impact their relative height, the densities are oppositely modified by $\Delta\rho$ such that the front and back intruders have a density $\rho \pm \Delta\rho$, respectively, where ρ is the density of the small particles. The aim is to quantify the impact on the longitudinal distance Δx . Second, the density of both intruders is reduced or increased identically, in the range $\rho_i \in [0.4\rho; 1.8\rho]$. Intruders will then locate either at the bottom, in the bulk, or at the surface of the granular flow, and this location should act on both Δz and Δx .

The configuration of two intruders with an intruder diameter $d_i = 10d$, a flow thickness $H = 15d$, a slope of 24° , and a rough incline made of small particles $d_r = d$ is considered again. Intruders are initially aligned ($\Delta y = 0$) and located at a longitudinal distance $\Delta x = 20d$ close to their equilibrium distance at this flow thickness.

Figure 18 shows the time evolution of the longitudinal distance Δx for the several density perturbations $\Delta\rho/\rho$. Positive values of $\Delta\rho/\rho$ correspond to a front intruder that is heavier

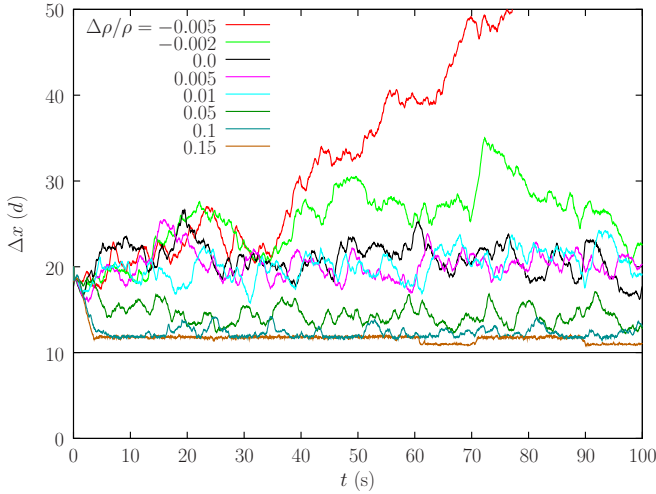


FIG. 18. Time evolution of the longitudinal distance Δx between two intruders of slightly different densities. Only the first 100 s are presented. The intruder size is $d_i = 10d$, the flow thickness is $H = 15d$, and the slope is $\theta = 24^\circ$. The density perturbation varies from $\Delta\rho/\rho = -0.005$ (front intruder lighter) to $\Delta\rho/\rho = 0.15$ (front intruder heavier). More intermediate cases have been simulated but are not presented for clarity.

and a back intruder that is lighter. The denser the front intruder is, compared to the back intruder, the closer are the intruders, showing an increase of the attracting effect. For the largest density modification $\Delta\rho/\rho = 0.15$, intruders are almost in contact with only one or two small particles in between them. The reverse situation is also considered with negative values of $\Delta\rho/\rho$ and a front intruder lighter than the back one. When the difference in density is not too large ($\Delta\rho/\rho = -0.002$, light-green curve), intruders remain in attractive interaction; however, the mean longitudinal length is larger ($\Delta x \simeq 30d$) showing a reduction of the attracting effect. When the density difference is further increased ($\Delta\rho/\rho = -0.005$, red curve), the longitudinal distance Δx continuously increases with time, and intruders escape from the mutual attraction. Figure 19 confirms the continuous decrease of the mean longitudinal distance between intruders $\langle\Delta x\rangle$ (red squares) when the density perturbation $\Delta\rho$ increases. In contrast, the associated mean height difference $\langle\Delta z\rangle$ (blue triangle, scale on right axis) evolves in a nonmonotonic way. It first increases and then decreases for $\Delta\rho/\rho \geq 0.06$. No significant variations in the height of the intruder center of mass ($\langle z_{CM}\rangle$, green dots) are observed in this range of $\Delta\rho$. The increase in the mean height difference (left part of the graph) can be deduced from the mean longitudinal distance by a horizontal mirror effect, as previously observed when varying the incline slope and roughness. On the other hand, the decrease in the mean height difference for $\Delta\rho/\rho \geq 0.06$ is reminiscent of the behavior observed when varying the flow thickness and assigned to the emergence of the intruders from the flow. Again, the interaction between the intruders proves not to be strong enough to maintain the vertical distance even though the intruders are close. In the second series of these numerical experiments, both intruders have the same density $\rho_i = \alpha\rho$ with the multiplying factor α in the range $[0.4; 1.8]$. As shown in Fig. 20,

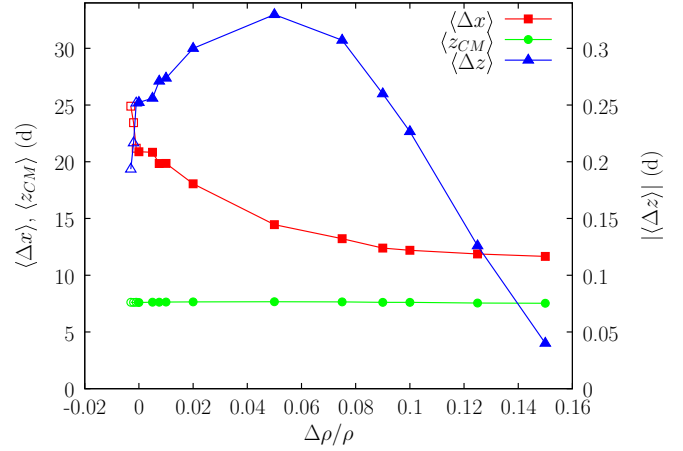


FIG. 19. Mean longitudinal distance $\langle\Delta x\rangle$ between intruders (red squares), mean height of the intruder center of mass $\langle z_{CM}\rangle$ (green dots), and the mean height difference between intruders $\langle\Delta z\rangle$ (blue triangles, scale on right axis) measured in small bead diameter (d) as a function of the density perturbation $\Delta\rho/\rho$. Empty symbols indicate values where $\Delta\rho/\rho < 0$.

this change in the intruder density alters the mean vertical position of the center of mass of the intruders ($\langle z_{CM}\rangle$) (green dots), as well as the mean longitudinal distance $\langle\Delta x\rangle$ (red squares) and height difference $|\langle\Delta z\rangle|$ (blue triangles, right axis) between intruders. Note that only the absolute value of the height difference is reported since negative values are encountered when intruders are so far apart (repulsive regime) that a front and a back intruders cannot be defined. Remarkably, changing the intruder density with respect to the small-particle density induces several regime transitions. Starting from the isodensity case $\rho_i/\rho = 1$, which corresponds to an attractive regime with a longitudinal distance $\langle\Delta x\rangle \simeq 20d$, and increasing the intruder density, the mean intruder height $\langle z_{CM}\rangle$ continuously

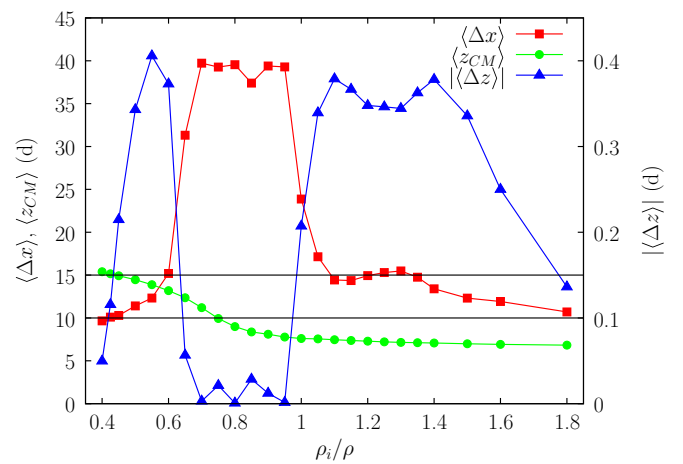


FIG. 20. Mean longitudinal distance $\langle\Delta x\rangle$ between intruders (red squares), mean height of the intruder center of mass $\langle z_{CM}\rangle$ (green dots), and absolute value of the height difference between intruders $|\langle\Delta z\rangle|$ (blue triangles, scale on right axis) measured in small bead diameter (d) as a function of the density ratio ρ_i/ρ . The dotted line indicates the free surface, and the dashed line indicates the height of intruders whose summit just emerges from the granular flow.

decreases, although more and more slowly, and saturates around $z \simeq 6.8d$: the intruders locate deeper in the flow, yet never touch the rough incline, even for the largest density ratio of 1.8. The longitudinal distance first reduces to $\langle \Delta x \rangle \simeq 15d$ where it reaches a plateau, up to $\rho_i/\rho = 1.4$, while the height difference increases up to around $\langle \Delta z \rangle \simeq 0.35d$. When the intruder density is further increased, $\langle \Delta x \rangle$ still decreases slightly and the height difference $\langle \Delta z \rangle$ strongly and continuously decreases. As in the case of a large difference in density between the intruders or a small flow thickness, the interaction between intruders whose density is much larger than that of the flowing small particles is no longer strong enough compared to their buoyancy to maintain the height difference.

Starting again at the value $\rho_i/\rho = 1$ and decreasing the intruder density, the mean intruder height $\langle z_{CM} \rangle$ continuously increases, i.e., the intruders locate higher and higher in the flow. Concomitantly, the longitudinal distance increases and shortly reaches its maximum possible value (for a numerical domain of length $L_x = 80d$), while the height difference $\langle \Delta z \rangle$ tends to zero; this corresponds to a repulsive regime. At a density $\rho_i/\rho \simeq 0.7$, only slightly smaller than the density for which the summits of the intruders emerge from the granular flow (dashed horizontal line at $z = 10d$ in Fig. 20), the intruders switch again to an attractive regime. The mean intruder height $\langle z_{CM} \rangle$ still increases, up to around $z \simeq 15.4d$ for the lowest density $\rho_i/\rho = 0.4$, for which the intruder centers are slightly above the free surface of the flow (dotted horizontal line at $z = 15d$). The longitudinal distance $\langle \Delta x \rangle$ continuously decreases until intruders are in contact. The height difference quickly increases, then decreases again at densities for which the intruder centers are very close to the free surface of the flow.

Two extra density ratios, $\rho_i/\rho = 0.35$ and 2, have been tested. For both of them, the back intruder is in contact with the front intruder and tries to overpass it. At some stage, the intruders are side by side, move away laterally from each other, and start flowing independently without interacting. No relative equilibrium position is reached and mean relative positions cannot be computed.

G. Link between vertical and longitudinal distances

Figure 21 reports all the numerical results on the longitudinal and vertical distances between intruders normalized by the intruder diameter d_i , for the size ratios $d_i/d = 9$ to 13. The rescaling by d_i is used to compare the data for different intruder sizes since the longitudinal and transverse distances between intruders are expected to depend mainly on the intruder diameter. Unless otherwise specified below, the parameter values are the following: domain size $L_x = 80d$, size ratio $d_i/d = 10$, flow thickness $H = 15d$, slope angle $\theta = 24^\circ$, incline roughness $d_r = d$, and isodensity for all particles $\rho_i = \rho$. For the size ratio $d_i/d = 10d$, data are reported for various density perturbations $\Delta\rho$ on the intruder densities and various densities ρ_i of both intruders, various flow thicknesses H for two domain sizes, and various incline slopes and roughnesses. Each couple $(\langle \Delta x \rangle, \langle \Delta z \rangle)$ was obtained by averaging over a period at least equal to 150 s, the first 50 s of the simulation being discarded to ensure convergence. The two black triangles in Fig. 21 stand for simulations where two horizontal springs are used to maintain nearly fixed the

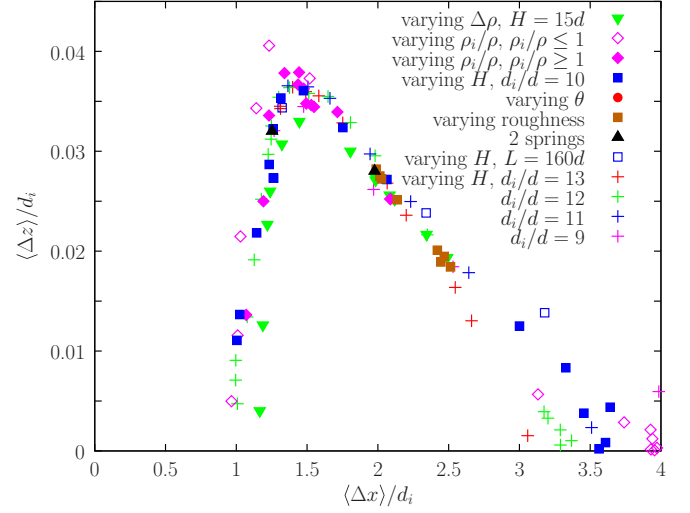


FIG. 21. Mean height difference $\langle \Delta z \rangle / d_i$ vs longitudinal distance $\langle \Delta x \rangle / d_i$ between intruders at equilibrium, with both quantities rescaled by the intruder diameter d_i . Except otherwise stated (label “varying”), the default parameters are $d_i/d = 10$, $H = 15d$, slope angle $\theta = 24^\circ$, incline roughness $d_r = d$, and isodensity $\rho_i = \rho$. For the size ratio $d_i/d = 10$, results are obtained by varying the density perturbation $\Delta\rho$ (green inverted triangles), the intruder density ($\rho_i/\rho \leq 1$: empty magenta diamonds, and $\rho_i/\rho \geq 1$: full magenta diamonds), the flow thickness H (blue filled squares for $L_x = 80d$ and blue empty squares for $L_x = 160d$), and the incline slope (red filled circles) and roughness (brown filled squares); the cases of intruders linked by two horizontal springs for $H = 15d$ and $9d$ (black filled triangles) are also reported. For the size ratios $d_i/d = 9, 11, 12$ and 13, the flow thickness H has been varied (colored plus symbols).

distances between the intruders and facilitate the computing of the velocity maps of the next section (see Sec. V). The data reported for the size ratios $d_i/d = 9, 11, 12$, and 13 have been obtained by varying the flow thickness H . The data for $d_i/d = 7, 8$, and 9 are not reported since they randomly fall around the master curve, due to the large fluctuations mentioned earlier.

The salient feature in Fig. 21 is that all of the data follow the same overall curve, no matter how they were obtained, i.e., data corresponding to the density perturbation $\Delta\rho$, obtained by changing the intruder density, resulting from the variations in H independently of the intruder diameter, and by changing θ and the incline roughness. In particular, in the case where both intruder densities are equal (filled and empty diamonds in Fig. 21), the curves superimpose independently of the fact that both intruders locate at the bottom of the flow when they are dense or near the free surface when they are light.

The right and left parts of the master curve of Fig. 21 show distinct behaviors. The right part reports systems where $\langle \Delta z \rangle$ decreases for increasing $\langle \Delta x \rangle$. The greater the distance between the intruders, the weaker their interaction, and, as expected, the height difference tends to zero. In contrast, the left part of the curve in Fig. 21 shows a positive correlation between $\langle \Delta x \rangle$ and $\langle \Delta z \rangle$. A decrease in $\langle \Delta z \rangle$ can result from several causes, i.e., a thin flow from which intruders emerge, a large intruder-density difference with a heavier front intruder, dense intruders that have a strong interaction with the rough

incline, or light intruders that emerge from the granular flow. All these also cause a decrease of $\langle \Delta x \rangle$. It is worth noting that the emergence of intruders from the granular flow causes their height difference Δz , which was usually increasing as intruders get closer, to decrease in a similar way whether the intruders emerge because the flow is thin or because their density is low.

For trial purposes, several simulations were performed on a longer simulation domain $L_x = 160d$ and various flow thicknesses (blue empty squares in Fig. 21). Although all the points fit with the master curve, a small deviation is observed at large values of the longitudinal distance $\langle \Delta x \rangle$, which correspond to the repelling regime and intruders far apart. Therefore, points corresponding to $\langle \Delta x \rangle$ typically larger than $30d$ should be considered only qualitatively, especially when obtained for the simulation domain of length $L_x = 80d$.

All the above highlights a tight link between the horizontal and vertical positions of two large intruders interacting in a granular flow.

V. A PROPOSED MECHANISM

When two particles are flowing in a fluid, for instance, spheres sedimenting in a liquid or cyclists, the back particle accelerates when in the wake of the front one. The situation is slightly more complex for intruders in a granular flow down an incline since they are in a shear flow. Intruders move faster than small particles flowing below them and slower than small particles flowing above them. To figure out the mechanisms at play in the interaction between intruders, an additional numerical experiment is performed, which aims at analyzing the velocity field of the granular flow in the neighborhood of the two intruders.

Parameters are set to their default values listed above. Intruders have a diameter $d_i = 10d$ and are fully embedded in a granular flow of thickness $H = 15d$, smaller than the transition thickness H^* but larger than the flow thickness for which the intruders start to emerge. Because the relative intruder positions Δx and Δy fluctuate with time, a specific procedure is necessary to reduce the amplitude of these fluctuations which would otherwise blur the measured velocity vector field around the intruders. This was achieved by adding two independent horizontal virtual springs between the intruders to force them to maintain their spacing at equilibrium [18]. The fluctuations on the vertical distance being rather small, no spring was added in the z direction. From Fig. 8, the no-load length is $\Delta x_0 = 20d$ for the spring aligned with the flow and $\Delta y_0 = 0$ for the transverse spring. The forces exerted by the virtual springs apply on the centers of the intruders and do not perturb their rotation. Their magnitudes are $k_x(\Delta x - \Delta x_0)$ and $k_y(\Delta y - \Delta y_0)$ in the x and y directions, respectively, where the spring stiffnesses, k_x and k_y , are chosen to keep the fluctuations around the equilibrium relative position smaller than $0.5d$. After test and trial, a value of $k_x = k_y = k_n/20\,000$ is retained, where k_n is the stiffness of the normal repulsion spring between any particles when in contact. Figure 22 reports the velocity field in the plane (Oxz) and the intruder positions in the reference frame of the front (right) intruder. The velocity field corresponds to the flow around two intruders being at their equilibrium relative position and is likely to

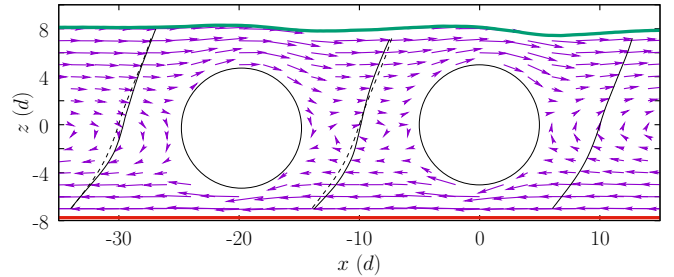


FIG. 22. Velocity map in the vertical plane in the reference frame (Oxz) of the front intruder (right intruder). The intruder size is $d_i = 10d$, the flow thickness is $H = 15d$, and the slope is $\theta = 24^\circ$. Intruders are at their relative equilibrium position: $\Delta x = 20d$ and $\Delta y = 0$. The thick green line stands for the free surface of the flow. The thick red line passes through the summit of the glued particles which form the rough incline. Three continuous inclined black lines indicate the velocity profile measured in front of the intruders (right black line), between them (middle black line), and behind them (left black line). The two inclined dashed lines duplicate the front velocity profile, shifted horizontally to facilitate comparison.

differ from the real velocity field around intruders that move out of equilibrium due to fluctuations. This nevertheless helps us to understand the involved mechanisms, as shown below. Furthermore, it can be noted that the height difference Δz computed for the intruders joined by two horizontal springs perfectly matches that of free intruders (see Fig. 21). This confirms that the springs are weak enough not to perturb the relative intruder positions when evaluating the velocity maps.

In Fig. 22 the thin black line around $x = -10d$ delineates the velocity profile between the two intruders while the thin black lines around $x = 10d$ and $x = -30d$ delineate the velocity profile ahead and behind the intruders, respectively. To facilitate comparison, the velocity profile at $x = 10d$ was reported between and behind the intruders (dashed lines at $x = -10d$ and $x = -30d$). This shows that, in the vertical direction and all over the diameter of the intruders, the velocity gradient is reduced between the intruders compared to that in front of the intruders. In the lower part of the flow $-5d \lesssim z \lesssim -d$, the velocities of small particles are larger than ahead of the front intruder; the lower half of the back intruder is in the wake of the lower half of the front intruder. The effect of this wake is to accelerate the back intruder until a new equilibrium position is reached. In the upper part of the flow $d \lesssim z \lesssim 5d$, the velocities of small particles between the two intruders are smaller than ahead of the front intruder and therefore than behind the back intruder since the two velocity profiles (front and back) are very close in the upper part of the flow (see Fig. 22); the upper half of the front intruder is in the wake of the upper half of the back intruder. The effect of this wake is to decelerate the front intruder. In brief, each intruder is in the wake of the other (in its upper or lower half), and both wakes push the intruders to get closer. Since the closer the intruders are, the higher the wake effect is, the velocity gradient in the region between them should further decrease and intruders should end up being in contact. However, an opposite mechanism causes the intruders to repel and derives from the height difference between the intruders. As they are embedded in a shear flow, the front intruder, which has

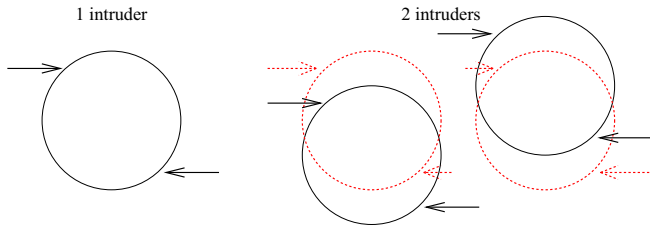


FIG. 23. Sketch of the intruder interactions with the small particles of the granular flow. The length of the arrows is indicative of the intensity of shocks with small particles. Red circles are reported positions of one single intruder to illustrate the asymmetry of shocks that would undergo two intruders having the same height. This asymmetry pushes the back intruder downwards and the front intruder upwards.

been measured higher in the flow, tends to go faster and the back intruder, which has been measured lower, tends to go slower. As a consequence, the intruders tend to move away from each other, increasing $\langle \Delta x \rangle$. These two mechanisms counterbalance to place intruders at a defined equilibrium distance. The origin of the height difference can be understood from Fig. 22. As discussed above, the wake effects experienced by the intruders are not symmetrical as they operate only on its lower part for the back intruder and only on its upper part for the front intruder. Figure 23 sketches the cases of one intruder (left) and of a couple of intruders (right) embedded in a granular shear flow. Intruders moving from left to right collide with small particles that are below them and move slower (bottom right arrows) and undergo collisions from small particles that are above them and move faster (top left arrow). The vertical location of an isolated intruder results from the equilibrium between the intruder weight, the buoyancy and the pressure induced by the collisions on the bottom-right and upper-left parts of the intruder. For two intruders at the same height (red dotted circles), the front intruder shields the lower flow for the back intruder, and the reverse happens for the upper flow on the front intruder. This dissymmetry disrupts the mechanism of vertical positioning, causing the front intruder to move upwards and the back intruder to move downwards, and new equilibrium positions are reached (black solid circles).

The emergence of the intruders above the free surface makes the picture more complex. Figure 24 is the counterpart

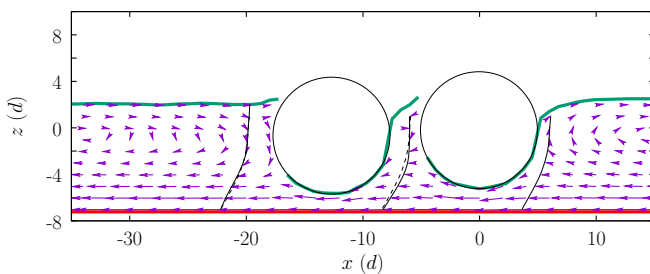


FIG. 24. Same as Fig. 22 except that the flow thickness is $H = 9d$. Intruders are at their relative equilibrium position: $\Delta x = 12.5d$ and $\Delta y = 0$. Intruders emerge from the free surface of the flow (thick green line).

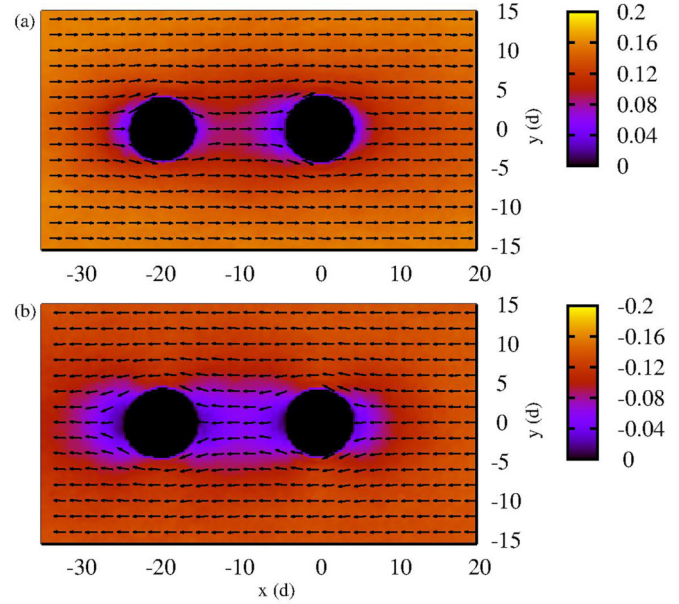


FIG. 25. Velocity map in the horizontal plane Oxy at a distance of $2.5d$ above (a) and below (b) the center of the front intruder in the reference frame of this intruder (right intruder). The intruder size is $d_i = 10d$, the flow thickness is $H = 15d$ and the slope is 24° . All vectors have the same length and the color map indicates the velocity amplitude in m/s.

of Fig. 22 for a flow thickness $H = 9d$. The length of the longitudinal spring equals the new equilibrium longitudinal distance between the intruders and is thus reduced to $\Delta x_0 = 12.5d$. Other parameters are unchanged. Figure 24 shows that the shear rate is reduced compared to the case $H = 15d$. This reduction is likely to reduce all wake effects and their attractive action. Concomitantly and as shown previously, the thinner the flow, the more the intruders emerge and the more the height difference between them is reduced by the additional buoyancy term. The repulsive effect in the flow direction due to the height difference reduces in turn. On the other hand, because there are fewer small particles, or none at all, flowing near the top of the intruders, the wake created by the upper part of the back intruder on the front intruder is reduced, as is its attractive effect. However, the absence of small particles flowing near the top of the intruders also means that small particles are no longer colliding with the summit of the back intruder, allowing it to locate higher in the flow. These two effects are opposed to each other, but as the latter reduction in Δz combines with the Δz reduction due to buoyancy, they may become dominant and counterbalance the reduction in the upper wake, inducing a smaller value of the longitudinal distance Δx . Finally, intruders reach equilibrium positions with a low Δx .

Another question that remains to be answered is why intruders align with the flow. Figure 25 shows two velocity maps in planes parallel to the incline and located half way between the center and the top of the front intruder [Fig. 25(a)] and half way between the center and the bottom of the front intruder [Fig. 25(b)], which corresponds to $z = 2.5d$ and $z = -2.5d$ in Fig. 22, respectively. The reference frame is that of the front intruder. The darker zones between the intruders show the

wake made by the back intruder in Fig. 25(a) and the wake made by the front intruder in Fig. 25(b). Note that Fig. 25 remarkably illustrates the difference in the amplitude of the wake effects felt by the intruders, likely due to the velocity gradient that characterizes the flow and to the vicinity of the rough incline. As soon as the front intruder is out of alignment, it is pushed back to the in-line position by the small particles that flow at the side of the intruders and that move faster than the small particles in the wake region of the back intruder [see the color code of Fig. 25(a)]. The counterpart situation is observed in the lower plane $z = -2.5d$, where the back intruder is in the wake of the front intruder [Fig. 25(b)]. In the attracting regime, intruders are close, the wakes are strong, and intruders perfectly align. When intruders are moving apart, they feel each other's wake less and less. In the steady state of the repulsive regime, intruders are unlikely to feel any wake. However, since they were initially close, they aligned during their separation, and a residual streamwise alignment remains visible. The pronounced transverse fluctuations observed may arise from the fluctuations in individual intruder trajectories.

VI. CONCLUSION

This paper reports experiments and DEM simulations on the interaction of two large particles in a flow of small particles down a rough incline. In the range of parameters explored, the two large particles, called intruders, do interact: they systematically align in the direction of the flow, while their longitudinal arrangement varies from intruders in contact to intruders far from each other. A difference in height of the intruders within the flow, with a tendency for the front intruder to rise and for the back intruder to sink, is also observed. The thorough parametric study performed reveals the existence of a master curve that links the equilibrium longitudinal distance between the intruders and their height difference in the flow. By means of simulations of the velocity field around the intruders, we demonstrate that the positions of two large particles in a dry granular flow on an incline result from a wake effect of each large particle on the other, combined with a vertical shear in the flow.

In many respects, the behaviors reported in this article and a few others (not presented here) observed, for example, during the transient stage are reminiscent of those exhibited by pairs of particles settling in fluids. Fully exploring the similarities and differences with the sedimentation of particles in a fluid medium is beyond the scope of this paper, but a few points are worth highlighting. The first obvious remark is

that a phenomenon analogous to the sedimentation in a fluid cannot take place in a granular material at rest, which behaves like a solid. The displacement of intruders requires movement of the small particles, a granular flow, for instance. Second, for shear flows, which are the most frequently encountered and the easiest to produce, two contrasting scenarios take place in connection with the speed of the intruders compared to that of the small particles. For thin flows where the intruders emerge, their velocity is higher than the mean flow velocity of the small particles, which present similarities to particles sedimenting in fluids. In contrast, when the flow is thick and intruders are fully immersed, they move at the velocity of the small particles flowing at the same height as they do. This makes the system closer to neutrally buoyant particles advected by a flow. Third, although two intruders not yet aligned with the granular flow (transient stage) have a lateral drift like in fluids, unlike particles sedimenting at low Reynolds number, they change their relative position by aligning with the flow and change their relative distance to reach a defined distance that depends on the flow thickness. Moreover, in the attracting regime at low flow thickness, intruders that are initially some distance apart end up in contact in a very similar way to the drafting and kissing observed at higher Reynolds number in the DKT phenomenon. In the case of very thin granular flows, the rear intruder tries to overtake the front intruder by passing it on one side, and, from time to time, the intruders lose contact, resembling the tumbling mechanism. Intruders end up in contact only after a more or less extended period of time. Finally, the alignment of the intruders in a granular flow is analogous to the one observed for particles or cyclists when flowing at higher Reynolds number. This highly interesting aspect of the similarities and differences in fluid and granular media certainly deserves further investigation.

This work also suggests that the interaction and alignment of large particles in polydisperse flows should break the homogeneity of the flow and induce the spontaneous formation of patterns, like trains of intruders or bands of large and small particles aligned with the flow. Such internal flow organizations can be of major interest in natural granular flows or industrial problems.

ACKNOWLEDGMENT

The Centre de Calcul Intensif d'Aix-Marseille University is acknowledged for granting access to its high-performance computing resources.

-
- [1] K. K. Rao and P. R. Nott, *An Introduction to Granular Flow* (Cambridge University Press, Cambridge, 2008).
 - [2] J. Duran, *Sands, Powders, and Grains: An Introduction to the Physics of Granular Materials* (Springer Science & Business Media, New York, 2012).
 - [3] B. Andreotti, Y. Forterre, and O. Pouliquen, *Granular Media: Between Fluid and Solid* (Cambridge University Press, 2013).
 - [4] J. M. Ottino and D. V. Khakhar, *Annu. Rev. Fluid Mech.* **32**, 55 (2000).
 - [5] E. Clement, J. Rajchenbach, and J. Duran, *Europhys. Lett.* **30**, 7 (1995).
 - [6] F. Cantelaube and D. Bideau, *Europhys. Lett.* **30**, 133 (1995).
 - [7] N. Thomas, *Phys. Rev. E* **62**, 961 (2000).
 - [8] G. Félix and N. Thomas, *Phys. Rev. E* **70**, 051307 (2004).
 - [9] N. Thomas and U. D'Ortona, *Phys. Rev. E* **97**, 022903 (2018).
 - [10] R. López de la Cruz and G. Caballero-Robledo, *J. Fluid Mech.* **800**, 248 (2016).

- [11] G. A. Caballero-Robledo, M. F. Acevedo-Escalante, F. Mandujano, and C. Málaga, *Phys. Rev. Fluids* **6**, 084303 (2021).
- [12] A. Tripathi and D. V. Khakhar, *Phys. Rev. Lett.* **107**, 108001 (2011).
- [13] K. van der Vaart, M. van Schroyen Lantman, T. Weinhart, S. Luding, C. Ancey, and A. Thornton, *Phys. Rev. Fluids* **3**, 074303 (2018).
- [14] L. Staron, *Phys. Fluids* **30**, 123303 (2018).
- [15] A. Kumar, D. V. Khakhar, and A. Tripathi, *Phys. Rev. E* **100**, 042909 (2019).
- [16] M. P. van Schroyen Lantman, K. van der Vaart, S. Luding, and A. R. Thornton, *Phys. Rev. Fluids* **6**, 064307 (2021).
- [17] A. V. Yennemadi and D. V. Khakhar, *Phys. Rev. Fluids* **8**, 074301 (2023).
- [18] F. Guillard, Y. Forterre, and O. Pouliquen, *J. Fluid Mech.* **807**, R1 (2016).
- [19] L. Jing, J. M. Ottino, R. M. Lueptow, and P. B. Umbanhowar, *Phys. Rev. Res.* **2**, 022069(R) (2020).
- [20] T. Trehwela, C. Ancey, and J. M. N. T. Gray, *J. Fluid Mech.* **916**, A55 (2021).
- [21] L. Jing, J. M. Ottino, P. B. Umbanhowar, and R. M. Lueptow, *J. Fluid Mech.* **948**, A24 (2022).
- [22] F. Pacheco-Vázquez and J. C. Ruiz-Suárez, *Nat. Commun.* **1**, 123 (2010).
- [23] D. D. Carvalho and E. M. Franklin, *Phys. Fluids* **34**, 123306 (2022).
- [24] M. Smoluchowski, *Bull. Acad. Sci. Cracovie A* **1**, 28 (1911).
- [25] M. Mason and W. Weaver, *Phys. Rev.* **23**, 412 (1924).
- [26] G. J. Kynch, *Trans. Faraday Soc.* **48**, 166 (1952).
- [27] J. F. Richardson and W. N. Zaki, *Trans. Inst. Chem. Eng.* **32**, S82 (1954).
- [28] J. Happel and H. Brenner, *Low Reynolds Number Hydrodynamics* (Prentice-Hall, 1965).
- [29] G. K. Batchelor, *J. Fluid Mech.* **52**, 245 (1972).
- [30] G. K. Batchelor, *J. Fluid Mech.* **119**, 379 (1982).
- [31] L. Durlofsky, J. F. Brady, and G. Bossis, *J. Fluid Mech.* **180**, 21 (1987).
- [32] J. F. Brady and G. Bossis, *Annu. Rev. Fluid Mech.* **20**, 111 (1988).
- [33] S. Kim and S. J. Karrila, *Microhydrodynamics: Principles and Selected Applications* (Butterworth-Heinemann, 2005).
- [34] A. Doostmohammadi and A. M. Ardekani, *Phys. Rev. E* **88**, 023029 (2013).
- [35] J. M. Crowley, *J. Fluid Mech.* **45**, 151 (1971).
- [36] J. M. Crowley, *Phys. Fluids* **19**, 1296 (1976).
- [37] R. Chajwa, N. Menon, S. Ramaswamy, and R. Govindarajan, *Phys. Rev. X* **10**, 041016 (2020).
- [38] A. Fortes, D. Joseph, and T. Lundgren, *J. Fluid Mech.* **177**, 467 (1987).
- [39] R. Sun and A. T. Chwang, *Phys. Rev. E* **76**, 046316 (2007).
- [40] J. Favier, A. Revell, and A. Pinelli, *J. Comput. Phys.* **261**, 145 (2014).
- [41] K. O. L. F. Jayaweera and B. J. Mason, *J. Fluid Mech.* **20**, 121 (1964).
- [42] B. Metzger, M. Nicolas and E. Guazzelli, *J. Fluid Mech.* **580**, 283 (2007).
- [43] A. El Yacoubi, S. Xu, and Z. J. Wang, *J. Fluid Mech.* **705**, 134 (2012).
- [44] J.-P. Matas, V. Glezer, E. Guazzelli, and J. F. Morris, *Phys. Fluids* **16**, 4192 (2004).
- [45] K. J. Humphry, P. M. Kulkarni, D. A. Weitz, J. F. Morris, and H. A. Stone, *Phys. Fluids* **22**, 081703 (2010).
- [46] S. Kahkeshani, H. Haddadi, and D. Di Carlo, *J. Fluid Mech.* **786**, R3 (2016).
- [47] C. Schaaf and H. Stark, *Eur. Phys. J. E* **43**, 50 (2020).
- [48] I. S. Santos de Oliveira, A. van den Noort, J. T. Padding, W. K. den Otter, and W. J. Briels, *J. Chem. Phys.* **135**, 104902 (2011).
- [49] P. A. Cundall and O. D. L. Starck, *Géotechnique* **29**, 47 (1979).
- [50] J. Schäfer, S. Dippel, and D. E. Wolf, *J. Phys. I France* **6**, 5 (1996).
- [51] U. D'Ortona, N. Thomas, and R. M. Lueptow, *Phys. Rev. E* **93**, 022906 (2016).
- [52] Z. Zaman, U. D'Ortona, P. B. Umbanhowar, J. M. Ottino, and R. M. Lueptow, *Phys. Rev. E* **88**, 012208 (2013).
- [53] N. Taberlet, M. Newey, P. Richard, and W. Losert, *J. Stat. Mech.* (2006) P07013.
- [54] P. Chen, J. M. Ottino, and R. M. Lueptow, *New J. Phys.* **13**, 055021 (2011).
- [55] G. H. Ristow, *Pattern Formation in Granular Materials* (Springer-Verlag, Berlin, 2000).
- [56] C. S. Campbell, *J. Fluid Mech.* **465**, 261 (2002).
- [57] L. E. Silbert, G. S. Grest, R. Brewster, and A. J. Levine, *Phys. Rev. Lett.* **99**, 068002 (2007).
- [58] See Supplemental Material at <http://link.aps.org/supplemental/10.1103/PhysRevE.109.064903> for Video 1: Simulation of a granular flow with two large intruders ($d_i/d = 10$). Periodic boundary conditions are applied in the x - y directions. The thickness of the flow is $H = 7d$ where d is the small particle diameter. Video 2: Same as video 1 with $H = 15d$. Video 3: Same as video 1 with $H = 18d$. Video 4: Experiment of a granular flow with two large intruders ($d_i/d \simeq 6$). The thickness of the flow is $H \simeq 6.5d$. Video 5: Same as video 4 with $H \simeq 8.5d$.
- [59] C. Goujon, N. Thomas, and B. Dalloz-Dubrujeaud, *Eur. Phys. J. E* **11**, 147 (2003).